OLiVia-Nav: An Online Lifelong Vision Language Approach for Mobile Robot Social Navigation

Siddarth Narasimhan **Aaron Hao Tan** **Daniel Choi** **Goldie Nejat**

Department of Mechanical and Industrial Engineering
University of Toronto, Canada

Abstract: In this paper, we present a novel Online Lifelong Vision Language architecture, OLiVia-Nav, which uniquely integrates vision-language models (VLMs) with an online lifelong learning framework for robot social navigation. We introduce a unique distillation approach, Social Context Contrastive Language Image Pre-training (*SC-CLIP*), to transfer the social reasoning capabilities of large VLMs to a lightweight VLM, in order for OLiVia-Nav to directly encode social and environment context during robot navigation. These encoded embeddings are used to generate and select robot social compliant trajectories. The lifelong learning capabilities of *SC-CLIP* enable OLiVia-Nav to update the lightweight VLM with robot trajectory predictions overtime as new social scenarios are encountered. We conducted extensive real-world experiments in diverse social navigation scenarios. The results showed that OLiVia-Nav outperformed existing DRL and VLM methods in terms of mean squared error, Hausdorff loss, and personal space violation duration. Ablation studies also verified our design choices.

Keywords: Social Navigation, Continual Learning, Vision Language Models

1 Introduction

Robot social navigation refers to the ability of an autonomous robot to move towards a goal within a human-centered environment while adhering to socially acceptable norms and behaviors [1]. Mobile service robots have been deployed in human spaces for tasks such as delivery of medication in hospitals [2], floor cleaning in office buildings [3], and patrolling for activity monitoring in long-term care facilities [4]. To promote safety and comfortability with humans while conducting such tasks, robots should navigate using social-awareness [5]. This includes respecting personal space [6], interpreting human movement intentions [7], and providing right of way to vulnerable people [8]. However, performing these social-aware actions can be challenging as robots must react to human behavior and contexts in real time [9], while dealing with varying social conditions [10].

Existing robot social navigation approaches have mainly used either human-model-based (HMB) [11]-[18] or human-model-free (HMF) [19]-[22], methods. In HMB methods, human trajectories are explicitly predicted and then incorporated into a navigation policy using deep reinforcement learning (DRL) [11]-[18]. HMF methods implicitly account for human trajectories by: 1) learning social navigation policies using imitation learning (IL) [19], [20], or 2) leveraging social reasoning capabilities of large foundation models such as large language models (LLMs) [21] or VLMs [22]. However, HMB and HMF methods do not account for social context, such as social scenarios that entail passing conversational groups or navigating against traffic, or environment context, such as open spaces versus narrow hallways. These contexts are important for robot path planning [22]. Furthermore, they are unable to adapt to new social scenarios (unexpected human behaviors, changes in the environment), resulting in degraded performance in real-world deployment [9].

In this paper, we present a novel **O**nline **Li**felong **Vi**sion L**a**nguage architecture, OLiVia-Nav, for mobile robot social navigation, which considers both social and environment context during robot

8th Conference on Robot Learning (CoRL 2024), Munich, Germany.

trajectory prediction and adapts to new social scenarios. OLiVia-Nav is the first architecture to leverage both the social reasoning capabilities of large VLMs, and the smaller size and faster response time of lightweight VLMs to generate social context embeddings of a robot's surroundings. Our main contributions are: 1) the development of a novel distillation process, *Social Context Contrastive Language Image Pre-training (SC-CLIP)*, that transfers the social reasoning capabilities of large VLMs into two lightweight encoders. These encoders extract social context embeddings from both visual and token semantic features from image and text captions, respectively, for predicting robot trajectories, and 2) the development of a trajectory prediction network that uniquely utilizes multi-head attention to account for these social context embeddings during the prediction of socially compliant robot trajectories. The encoders support online lifelong learning to adapt to new unseen social navigation scenarios during robot navigation.

2 Related Works

Existing approaches can be categorized into: 1) human-model-based (HMB) methods [11]-[18], 2) human-model-free (HMF) methods [19]-[22], and 3) lifelong learning methods [23], [24].

Human-Model Based Methods (HMB). In general, HMB methods predict the trajectories of people in the robot's surrounding and then learn a robot social navigation policy that accounts for these predicted trajectories. Human trajectories have been predicted using constant velocity (CV) models [16], transformer models [11], [13], [18], or human tracking (HT) models [12], [14], [15] using RGB images and LiDAR point clouds. In CV models, human trajectories are predicted by assuming a constant speed and direction [16]. In transformer models, a spatial-temporal graph transformer is used to encode distance relationships between people overtime to predict their positions [11], [13], [18]. Lastly, HT models utilize tracker methods such as YOLO [25] to detect and track human positions using either bounding boxes [12], [15] or LiDAR point clouds [14]. These models then predict trajectories by estimating velocity and direction from the tracked human positions. The predicted trajectories are then used to generate social navigation policies by using DRL methods [11], [13], [14], [16]-[18] or heuristic control methods [12], [15]. Namely, DRL techniques include actor-critic [11], [14], proximal policy optimization (PPO) [13], [16], [17], and double deep Q network [18], which optimize reward functions to maximize personal space and minimize collisions. Heuristic control policy methods consist of predefined rules used to generate policies to avoid human trajectories [12], [15]. The HMB methods are trained using 2D simulated environments, where humans are represented as point masses [11], [12], [14] [16], [18], or 3D simulated environments with procedurally generated human trajectories [13], [17].

Human-Model Free Methods (HMF). HMF methods consist of: 1) imitation learning (IL) methods [19], [20] which learn social navigation policies from expert knowledge in datasets, or 2) large foundation model methods (e.g., LLMs/VLMs) [21], [22]), that generate robot actions based on their social reasoning capabilities. IL methods use behavior cloning [19] or transformer architectures [20] to predict robot trajectories. They have leveraged social navigation datasets such as SCAND [26], MuSoHu [27] and THOR-Magni [28], which contain expert demonstrations of robot trajectories from real-world environments. LLMs and VLMs exhibit social reasoning capabilities as they are pre-trained on internet-scale data [29]. These methods generate social navigation policies in two stages. Firstly, LLMs and VLMs are prompted to generate social and environment context captions using audio [21] or image [22] inputs. Secondly, a navigation planner (DRL [21] or the dynamic window approach (DWA) [22]) use these captions to generate socially compliant navigation actions.

Lifelong Learning Methods. Lifelong learning methods incrementally update navigation model parameters to adapt to new social scenarios overtime, and have only been applied to HMB methods [23], [24]. For example, in [23], human trajectories were first tracked using a Kalman filter (KF) with visual and LiDAR data to estimate their positions and velocities. Lifelong learning was achieved by updating probability distribution maps with this tracking data, predicting human positions relative to the robot at discrete future time steps. In [24], a DRL architecture using PPO was trained with the THOR-Magni dataset [28] to predict human trajectories using gated recurrent units (GRUs). The predicted trajectories were used to quantify deviations from socially acceptable behaviors through a

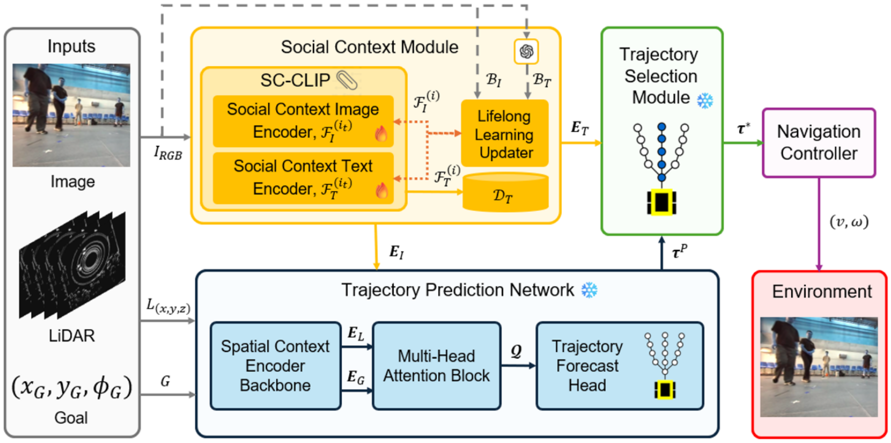

Figure 1: OLiVia-Nav consists of four modules, 1) *Social Context Module (SCM)* extracts social context embeddings for trajectory prediction and selection, and to update the social context image and text encoders for lifelong learning, 2) *Trajectory Prediction Module (TPM)* generates socially compliant navigation trajectories using LiDAR data, goal and the social context image embedding, 3) *Trajectory Selection Module (TSM)* selects the trajectory that follows the high-level navigation action encoded in the social context text embedding, and 4) *Navigation Controller (NC)* uses a Proportional Integral Derivative (PID) controller to follow the selected trajectory.

social cost function, which was incorporated into the DRL reward function. The lifelong learning process continuously updated the weights for the navigation policy by retraining the model with new human interaction data collected during navigation.

Summary of Limitations. HMB methods cannot account for social and environmental context in real-world scenarios [11]-[18]. Lifelong learning approaches using HMB rely on predefined human motion models in a KF, which lack visual cues and human behavior integration [23]. Additionally, these methods face sim-to-real gaps due to reliance on simulation-based datasets [24]. HMF methods using IL [19], [20] are restricted to the social scenarios present in their training data, which limits generalization to unseen real-world scenarios [26]. LLMs and VLMs are constrained by slow response times, leading to delayed adaptation to dynamic human movements and increased risk of collisions [30]. To address these limitations, OLiVia-Nav: 1) leverages *SC-CLIP* to generate social context embeddings that encode the robot's environment, human behavior, and high-level navigation for trajectory prediction and selection, and 2) incorporates online lifelong learning with lightweight *SC-CLIP* encoders that update during navigation to adapt to new, unseen social scenarios.

3 Robot Social Navigation Problem

Robot social navigation addresses the problem of a mobile robot that needs to navigate from its initial pose (x_0, y_0, ϕ_0) to a goal pose (x_G, y_G, ϕ_G) in an unknown environment consisting of dynamic people. The robot uses RGB images from its onboard camera, I_{RGB}, to detect visual features such as people and objects, and 3D LiDAR point clouds, $L_{(x,y,z)}$, to provide the 3D structural layout of the robot's surrounding. The task is to predict K socially compliant future trajectories, $\boldsymbol{\tau}^P$, from (x_0, y_0, ϕ_0) to (x_G, y_G, ϕ_G) given an expert demonstration trajectory $\boldsymbol{\tau}^E = \{(x_j, y_j, \phi_j)\}_{j=0}^{G}$:

$$\boldsymbol{\tau}^P = \left\{ \tau_k^P : \tau_k^P = \left\{(x_i^k, y_i^k, \phi_i^k)\right\}_{i=0}^{G}, k \in [1, K] \right\}. \tag{1}$$

The trajectories, $\boldsymbol{\tau}^P$, are generated by a deep neural network, $f_\theta(I, L)$ with learnable parameters, θ. The overall objective is to learn θ in order to minimize the winner-takes-all (WTA) loss [31] between the predicted and expert trajectories:

$$\theta^* = \arg\min_{\theta} \mathrm{WTA}(f_\theta(I, L), \boldsymbol{\tau}^E). \tag{2}$$

4 OLiVia-Nav Architecture

The OLiVia-Nav architecture consists of four main modules, Fig. 1: 1) *Social Context Module (SCM)*, 2) *Trajectory Prediction Network (TPN)*, 3) *Trajectory Selection Module (TSM)*, and 4) *Navigation Controller (NC)*.

4.1 Social Context Module (SCM)

The proposed *SCM* consists of two submodules: 1) *Social Context Contrastive Language Image Pretraining (SC-CLIP)*, and 2) a *Lifelong Learning Updater (LLU)*, Fig. 1.

Social Context Contrastive Language Image Pretraining (SC-CLIP). We introduce *SC-CLIP*, a distillation approach to transfer the social reasoning of a large VLM to two lightweight encoders: a social context image encoder (*SCIE*), $\mathcal{F}_I$, and a social context text encoder (*SCTE*), $\mathcal{F}_T$. The novelty of *SC-CLIP* is its ability to retain the social understanding of a large VLM, enabling OLiVia-Nav to generalize to diverse social scenarios, without the slow response speed of the large VLM.

The distillation approach consists of two stages. First, a large VLM is used to generate a long and short text caption, (T_l, T_s), to describe the social and environment context within I_{RGB}, Fig. 2. This context includes descriptions of: 1) the social scenario, 2) objects and people in the environment, and 3) the high-level navigation action that the robot should follow to remain socially compliant. Then, in the second stage, *SC-CLIP* trains the $\mathcal{F}_I$ and $\mathcal{F}_T$ in parallel to align the image embedding, $\boldsymbol{E}_I$, from I_{RGB}, with the corresponding text embedding, $\boldsymbol{E}_T$, from (T_l, T_s), in their respective embedding spaces. Herein, $\mathcal{F}_I$ utilizes a ViT-L/14 transformer backbone [32] to extract visual semantic features from I_{RGB} in order to generate $\boldsymbol{E}_I$. $\mathcal{F}_T$ utilizes a self-attention transformer backbone [33] to extract token semantic features from (T_l, T_s) to generate $\boldsymbol{E}_T$. *SC-CLIP* is trained using the following loss function [34]:

$$\mathcal{L}_{SC-CLIP} = \mathrm{CE}(\mathcal{F}_I(I_{RGB}) \cdot \mathcal{F}_T(T_l)^T, labels) + \mathrm{CE}(\mathrm{PCE}(\mathcal{F}_I(I_{RGB})) \cdot \mathcal{F}_T(T_s)^T, labels), \tag{3}$$

where PCE is the Principal Component Extraction function, which extracts high-level context features from $\mathcal{F}_I(I_{RGB})$ [35], CE is the cross-entropy loss, and $labels$ are the ground truth indices that align $\boldsymbol{E}_I$ and $\boldsymbol{E}_T$.

The trained $(\mathcal{F}_I, \mathcal{F}_T)$ are used to incorporate social and environmental context to be used for trajectory prediction and selection. Specifically, $\mathcal{F}_I$ is used to generate $\boldsymbol{E}_I$, from RGB images as the robot navigates an environment. $\mathcal{F}_T$ is used to create $\mathcal{D}_T$, of size $|\mathcal{D}_T|$, from an offline dataset (discussed in Section V). During navigation, $\boldsymbol{E}_I$ is used for: 1) trajectory prediction by *TPN*, and 2) retrieving $\boldsymbol{E}_T$ from $\mathcal{D}_T$ based on a cosine similarity score, for trajectory selection by *TSM*.

Lifelong Learning Updater (LLU). The objective of the *LLU* is to update $\mathcal{F}_I$ and $\mathcal{F}_T$ during robot navigation to account for new social scenarios that were not present during training. *LLU* collects a batch, $\mathcal{B}_I$, of I_{RGB} during navigation and stores the batch in a buffer of size $|\mathcal{B}|$. These images are passed to a large VLM to obtain the batch, $\mathcal{B}_T$, which is also used to update $\mathcal{F}_I$ and $\mathcal{F}_T$. A Symmetric Image-Text fine-tuning strategy is used for the loss function [36]:

$$\mathcal{L}_{\mathcal{LLU}} = -\sum_{\boldsymbol{E}_I \in V_I} \log \frac{\exp\left(\frac{\mathcal{K}(\boldsymbol{E}_I, \boldsymbol{E}_T)}{\mu}\right)}{\sum_{\boldsymbol{E}'_T \in V_T} \exp\left(\frac{\mathcal{K}(\boldsymbol{E}_I, \boldsymbol{E}'_T)}{\mu}\right)}, \tag{4}$$

where V_I are image features from batch $\mathcal{B}_I$, and V_T are the text features from the batch $\mathcal{B}_T$, $\mathcal{K}(\cdot,\cdot)$ measures the cosine similarity score, and μ is the temperature to control the sharpness of the distribution. We denote $\mathcal{F}_I$ at update iteration i, as $\mathcal{F}_I^{(i)}$, and $\mathcal{F}_T$ at iteration i, as $\mathcal{F}_T^{(i)}$. The last iteration is denoted as $\mathcal{F}_I^{(i_t)}$ and $\mathcal{F}_T^{(i_t)}$, where i_t represents the latest *LLU* iteration update. The updated encoders, $\mathcal{F}_I^{(i_t)}$ and $\mathcal{F}_T^{(i_t)}$, are used to generate $\boldsymbol{E}_I$ and $\mathcal{D}_T$, respectively.

4.2 Trajectory Prediction Network (TPN)

We propose a novel *TPN* to generate socially compliant trajectory candidates, $\boldsymbol{\tau}^P$, by uniquely incorporating LiDAR data $L_{(x,y,z)}$, navigation goal $G = (x_G, y_G, \phi_G)$, and the social context embed-

Long Text Caption (T_l): In the provided image, the scenario involves navigating among dynamic people in a shopping area. There are several people present, including a person in an orange jacket walking ahead and slightly to the left, and another person in a red jacket standing near a flower planter on the right in the immediate vicinity. The pathway is clear, but it curves slightly to the right. To navigate safely, you should continue moving straight while gradually turning to the right to follow the pathway. Ensure to maintain a safe distance from the person in the orange jacket and avoid any sudden movements that could cause collisions.

Short Text Caption (T_s): People in orange and red jackets walking and standing in a busy shopping area. Curving pathway with flower planter on the right.

Figure 2: Example of a long and short text caption generated by the large VLM for training SC-CLIP. The long text caption describes the social scenario, objects and people in the environment and the high-level navigation action for the robot. The short text caption is a summary of the long-text caption. Image is from the MuSoHu dataset [27].

ding, $\boldsymbol{E}_I$. The *TPN* consists of a spatial context encoder backbone (*SCEB*), a multi-head attention block (*MHAB*), and a trajectory forecast head (*TFH*), Fig. 1.

The *SCEB* consists of two encoders. A LiDAR encoder to extract voxel features for the 3D points residing in each voxel [37] using five residual blocks [38] in order to obtain the LiDAR embedding vector, $\boldsymbol{E}_L$. A goal encoder uses a single layer feed-forward network (FFN) and rectified linear unit (ReLU) activation to obtain the goal embedding vector, $\boldsymbol{E}_G$. $\boldsymbol{E}_L$, $\boldsymbol{E}_G$ and $\boldsymbol{E}_I$ are fused together using the *MHAB* to exchange context-relevant information across each embedding representation. The attention process starts with a randomly initialized query, $\boldsymbol{\mathcal{Q}}^{(0)}$, which passes through three cross-attention layers: 1) *SC-CLIP* cross-attention to incorporate social and environment context from I_{RGB}, 2) LiDAR cross-attention to incorporate geometric and motion features from $L_{(x,y,z)}$, and 3) goal cross-attention to condition the trajectory generation on G. Each attention block updates the query sequentially using [39]:

$$\boldsymbol{\mathcal{Q}}^{(z)}_{att} = \text{LN}\left(\boldsymbol{\mathcal{Q}}^{(z)} + \mathcal{A}(\boldsymbol{\mathcal{Q}}^{(z)}, \cdot)\right), \tag{5}$$

$$\boldsymbol{\mathcal{Q}}^{(z+1)} = \text{LN}\left(\boldsymbol{\mathcal{Q}}^{(z)}_{att} + \text{FFN}(\boldsymbol{\mathcal{Q}}^{(z)}_{att})\right), \tag{6}$$

where $\boldsymbol{\mathcal{Q}}^{(z)}_{att}$ represents the intermediate query after performing cross-attention on the z^{th} attention layer, $\boldsymbol{\mathcal{Q}}^{(z)}$ represents the query for the z^{th} attention layer, $\mathcal{A}$ represents the cross-attention operations, LN denotes layer normalization. The final output, $\boldsymbol{\mathcal{Q}}^{(3)} = \boldsymbol{\mathcal{Q}}$, is passed into the *TFH* for trajectory prediction.

In the *TFH*, the output query is fed into N_{GRU} GRUs with each predicting one trajectory, τ^P_k. The outputs are concatenated into a single vector, $\boldsymbol{\tau}^P$, Eq. 1. The *TPN* is trained using the WTA loss function, Eq. 2, to predict multiple trajectories. The *TSM* then uses $\boldsymbol{\tau}^P$ for trajectory selection.

4.3 Trajectory Selection Module (TSM)

The objective of the *TSM* is to select a socially compliant trajectory from $\boldsymbol{\tau}^P$ using $\boldsymbol{E}_T$. Namely, $\boldsymbol{E}_T$ is passed through an FFN to produce $\boldsymbol{E}_\tau$, while $\boldsymbol{\tau}^P$ is processed by a separate FFN and GRU to produce embedding vector $\boldsymbol{E}_C$. The *TSM* is trained using the following loss function:

$$\mathcal{L}_{TSM} = \text{CE}(\text{FFN}(\boldsymbol{E}_C \oplus \boldsymbol{E}_\tau), k^*), \tag{7}$$

where $\oplus$ represents the concatenation operation and k^* is an index identifies the trajectory, $\boldsymbol{\tau}^*$, that is described by the navigation action in T_l. $\boldsymbol{\tau}^*$ is used by the *NC* for execution.

4.4 Navigation Controller (NC)

The selected $\boldsymbol{\tau}^*$, is used by *NC* to generate robot velocities, (v, ω) using a PID controller [40].

5 Datasets

We collected three datasets to train the modules of OLiVia-Nav: 1) Social Context Dataset, $\mathcal{D}_{SC}$, using images from MuSoHu [27] to train *SC-CLIP*, 2) Trajectory Prediction Dataset, $\mathcal{D}_{TPN}$, using expert trajectories, LiDAR point clouds and RGB images from MuSoHu to train the *TPN*, and 3) Trajectory Selection Dataset, $\mathcal{D}_{TSM}$, using expert trajectories from MuSoHu to train the *TSM*.

Social Context Dataset, $\mathcal{D}_{SC}$. This dataset comprises of 20,000 RGB images, and corresponding (T_l, T_s), which are generated using GPT4o [30]. We use GPT4o for its ability to generate socially related and contextually relevant captions [41]. The text captions include descriptions of the social scenario, objects and people in the scene, and the high-level navigation plan. The database, $\mathcal{D}_T$, used within the *LLU*, is curated by taking a randomized subset of T_l from $\mathcal{D}_{SC}$, and generating the corresponding $\boldsymbol{E}_T$ using $\mathcal{F}_T^{(i_t)}$.

Trajectory Prediction Dataset, $\mathcal{D}_{TPN}$. This dataset comprises of 5,000 expert trajectories, LiDAR point clouds, and RGB images. The expert trajectories, $\boldsymbol{\tau}^E$, are represented by a sequence of 10 future robot poses $\left\{(x_i^E, y_i^E, \theta_i^E)\right\}_{i=0}^{10}$ from the current robot pose. For each sequence, all waypoints are transformed into the reference frame of the initial robot pose, $(x_0^E, y_0^E, \theta_0^E)$, for normalization and consistency in prediction outputs. I_{RGB}, is taken at the robot's initial pose.

Trajectory Selection Dataset, $\mathcal{D}_{TSM}$. This dataset consists of 20,000 predicted trajectories, $\boldsymbol{\tau}^P$, along with the corresponding RGB images, I_{RGB}, T_l, $\boldsymbol{E}_T$, and the trajectory index, k^*, that corresponds to the high-level action in T_l.

6 Training

OLiVia-Nav was trained in three stages: 1) *SCIE* and *SCTE* using the *SC-CLIP* framework, Eq. 3, 2) *TPN* in an end-to-end manner, Eq. 2, and 3) *TSM* based on the predictions of the *TPN*, Eq. 5 and 6. Training was conducted with NVIDIA H100 GPU with 80GB of VRAM and 32GB of RAM.

SC-CLIP Training. *SC-CLIP* was trained with a batch size of 256 and a cosine annealing learning rate scheduler with a learning rate (LR) of 0.0001 [42], to gradually reduce LR over time for convergence. An AdamW optimizer [43] was used with weight decay (WD) of 0.01 to prevent overfitting. *SC-CLIP* was trained for 100 epochs.

TPN Training. The *TPN* was trained with a batch size of 10, LR of 0.0008, and the AdamW optimizer with WD 0.0001. $\boldsymbol{E}_I$, $\boldsymbol{E}_T$ and $\boldsymbol{E}_G$ were projected into a common dimension of $C = 128$ using an FFN. For *MHAB*, 32 heads were used. The number of predicted trajectories was set to $K = 5$, and correspondingly $N_{GRU} = 5$. *TPN* was trained for 500 epochs.

TSM Training. The *TSM* was trained with a batch size of 128 and an LR of 0.00001. A WD of 0.00001 was used with an AdamW optimizer. *TSM* was trained for 500 epochs similar to *TPN*.

7 Experiments

We conducted two sets of experiments in: 1) a real-world comparison study with state-of-the-art (SOTA) social navigation methods, and 2) an ablation study to investigate the design choices of OLiVia-Nav. We used GPT4o [30] as the large VLM within the *SCM*.

7.1 Comparison Study

Three metrics were used: 1) mean squared error (MSE) for positional error, 2) Hausdorff loss [44] for trajectory shape similarity, and 3) personal space violation duration (PSV) for time spent within 0.25 m of a person [45]. Ground truth trajectories were collected via teleoperation. Four social scenarios with 3 trials each were tested: 1) narrow hallway, Fig. 3(a), 2) blind corner, Fig. 3(b), 3) navigating static groups, Fig. 3(c), and 4) dynamic groups, Fig. 3(d), similar to [26].

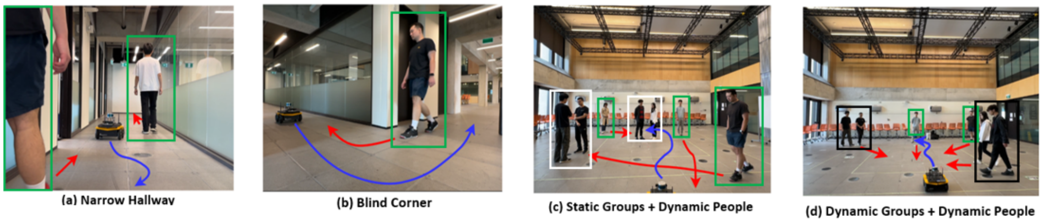
(a) Narrow Hallway

(b) Blind Corner

(c) Static Groups + Dynamic People

(d) Dynamic Groups + Dynamic People

Figure 3: The four experimental scenarios: (a) narrow hallway, (b) blind corner, (c) static groups + dynamic people, and (d) dynamic groups + dynamic people. Red arrows show human trajectories, blue arrows show the robot's predicted path, and green, white, and black boxes represent dynamic people, static groups, and dynamic groups, respectively.

Table 1: Comparison Results for the Four Social Scenarios

Scenario	**Method**	**MSE ↓**	**Haus ↓**	**PSV (s) ↓**
Narrow Hallway	**OLiVia-Nav**	**0.1075**	**0.7348**	**1.2**
	VLM-Social-Nav	0.1915	0.8785	1.9
	MultiSoc	0.2968	0.9095	2.1
Blind Corner	**OLiVia-Nav**	**0.0236**	**0.2572**	**0.4**
	VLM-Social-Nav	0.0755	0.5384	2.6
	MultiSoc	0.1021	0.4596	2.8
Static Groups + Dynamic People	**OLiVia-Nav**	**0.2195**	**0.7563**	**2.1**
	VLM-Social-Nav	0.4361	1.5579	3.5
	MultiSoc	0.2747	1.1081	3.2
Dynamic Groups + Dynamic People	**OLiVia-Nav**	**0.0733**	**0.4813**	**3.3**
	VLM-Social-Nav	0.1459	0.6832	4.7
	MultiSoc	0.1154	0.7929	4.5

↓ indicates that lower values are better.

Comparison Methods. We benchmarked OLiVia-Nav against the following SOTA methods: **1) VLM-Social-Nav** [22]. This HMF approach uses a cost-based planner with GPT4o for social navigation. Costs include 1) obstacle collision from LiDAR, 2) goal position, and 3) social cost from RGB images via GPT4o. The planner selects the lowest-cost velocity pair (v, ω). We choose VLM-Social-Nav to assess how GPT4o affects navigation performance, considering its slower response time; and **2) MultiSoc** [16]. This HMB method uses a GNN with attention mechanisms to predict human trajectories by processing RGB images and LiDAR data. These predictions are integrated into a DRL navigation policy trained with proximal policy optimization [46], outputting robot velocity commands (v, ω). We choose MultiSoc to benchmark OLiVia-Nav as it is trained in a 2D simulator with hand-crafted human trajectories, allowing comparison with our method that uses real-world human trajectories.

Results. The results of the comparison study are presented in Table I. OLiVia-Nav had the lowest MSE, Hausdorff loss, and PSV across all scenarios, generating social navigation trajectories that closely match ground truth trajectories in both proximity and shape. OLiVia-Nav utilizes the TPN, which was trained using IL on a dataset containing real-world human trajectories and diverse environments. This enabled OLiVia-Nav to predict robot trajectories that resemble human navigation behaviors in realistic social scenarios [9]. In contrast, VLM-Social-Nav utilized hand-tuned cost functions to generate robot trajectories for obstacle avoidance and goal reaching instead of real-world data. This approach limited the VLM-Social-Nav's ability to adapt to nuanced real-world behaviors, such as a robot dynamically adapting its speed and orientation when navigating around a corner. As a result, VLM-Social-Nav had lower performance than OLiVia-Nav. Lastly, MultiSoc resulted in robot navigations that had frequent heading direction changes, since social and environment context were not explicitly incorporated during training [16].

Table 2: Ablation Study

	Before *LLU* Update		After *LLU* Update	
Methods	**MSE** $\downarrow$	**Haus.** $\downarrow$	**MSE** $\downarrow$	**Haus.** $\downarrow$
OLiVia-Nav (ours)	**0.2981**	**1.8087**	**0.2521**	**1.4893**
OLiVia-Nav w/o $\boldsymbol{E}_I$	0.4412	2.3772	0.3701	2.0839
OLiVia-Nav w/o $\boldsymbol{E}_T$	0.3838	2.1063	0.3791	2.0349
OLiVia-Nav w/o $\boldsymbol{E}_L$	0.4382	2.3681	0.4180	2.1894
OLiVia-Nav w/o $\boldsymbol{E}_G$	0.5991	3.1072	0.5393	2.8648

$\downarrow$ indicates that lower values are better.

In general, OLiVia-Nav demonstrated lower PSV than both VLM-Social-Nav and MultiSoc. VLM-Social-Nav had a higher PSV due to its slower response speed ($\sim$0.6Hz), compared to OLiVia-Nav ($\sim$5Hz), as it relied on querying GPT4o to compute social costs. This caused delays in executing navigation actions which resulted in longer durations of personal space violations. Although MultiSoc can plan in real time ($\sim$5Hz), it exhibited a higher PSV compared to OLiVia-Nav due to inaccurate human trajectory predictions. Namely, MultiSoc frequently changed the robot's heading direction in response to pose errors in the predicted human trajectories, which resulted in the robot violating personal space. A video is on our YouTube channel: https://youtu.be/wp9BqxHESTk .

7.2 Ablation Study

We considered: 1) **OLiVia-Nav without (w/o) $\boldsymbol{E}_I$** to determine the effect of visual semantic features from I_{RGB} on trajectory prediction in the *TPN*, 2) **OLiVia-Nav w/o $\boldsymbol{E}_T$** to evaluate the impact of token semantic features from (T_l, T_s) on the selected trajectory in *TSM*, 3) **OLiVia-Nav w/o $\boldsymbol{E}_L$** to explore the influence of the LiDAR point cloud embedding on trajectory prediction, and 4) **OLiVia-Nav w/o $\boldsymbol{E}_G$** to explore the contribution of goal embeddings on trajectory prediction.

For each of these variants, the performance was evaluated twice; Before *LLU* Update, using only $\mathcal{F}_I^{(0)}$ and $\mathcal{F}_T^{(0)}$, and After *LLU* Update, using $\mathcal{F}_I^{(i_t)}$ and $\mathcal{F}_T^{(i_t)}$, where $i_t = 1$. The goal is to investigate the contribution of the *LLU* on all variants in terms of adapting to new social scenarios. Our results for lifelong learning were obtained using a hold-out test dataset in MuSoHu.

Results. The ablation study results are presented in Table II. The Before *LLU* Update results show that the OLiVia-Nav had the lowest MSE and Hausdorff loss compared to all variants. The After *LLU* Update results also showed OLiVia-Nav having the lowest MSE and Hausdorff loss of 0.2521 and 1.4893, respectively. All ablation variants also improved their performance with the updates. For example, OLiVia-Nav w/o $\boldsymbol{E}_I$ achieved a higher MSE and Hausdorff loss compared to OLiVia-Nav as the predicted robot trajectories did not consider social and environment context. OLiVia-Nav w/o $\boldsymbol{E}_T$ also achieved degraded navigation performance as the variant was unable to utilize high-level action information from this embedding, resulting in the random selection of trajectories. As OLiVia-Nav w/o $\boldsymbol{E}_L$ did not the use the LiDAR embedding, trajectory predictions resulted in collisions with people. Lastly, OLiVia-Nav w/o $\boldsymbol{E}_G$ achieved the lowest performance since this variant did not use navigation goals. This prevented the robot from arriving at its desired goal pose.

8 Conclusion

In this paper, we present a novel lifelong vision language architecture OLiVia-Nav which uses VLMs to address the robot social navigation problem in dynamic human environments. Our approach introduces a novel distillation process, *SC-CLIP*, to leverage the social reasoning capabilities of large VLMs for trajectory prediction while being able to adapt online to new scenarios using the lifelong learning ability of the lightweight VLM. Extensive real-world experiments demonstrate that OLiVia-Nav follows expert trajectories more accurately compared to SOTA methods. Furthermore, ablation studies show the importance of each of the embeddings on robot social navigation performance. Future work will investigate the performance of the OLiVia-Nav in larger environments with crowds.

References

[1] A. Francis et al., “Principles and Guidelines for Evaluating Social Robot Navigation Algorithms,” Sep. 19, 2023, arXiv: arXiv:2306.16740. Accessed: Jun. 18, 2024. [Online]. Available: http://arxiv.org/abs/2306.16740

[2] A. A. Morgan, J. Abdi, M. A. Q. Syed, G. E. Kohen, P. Barlow, and M. P. Vizcaychipi, “Robots in Healthcare: a Scoping Review,” Curr Robot Rep, vol. 3, no. 4, pp. 271–280, Oct. 2022, doi: 10.1007/s43154-022-00095-4.

[3] R. Memmesheimer et al., “Cleaning Robots in Public Spaces: A Survey and Proposal for Benchmarking Based on Stakeholders Interviews,” Jul. 23, 2024, arXiv: arXiv:2407.16393. Accessed: Sep. 15, 2024. [Online]. Available: http://arxiv.org/abs/2407.16393

[4] C. Getson and G. Nejat, “Socially Assistive Robots Helping Older Adults through the Pandemic and Life after COVID-19,” Robotics, vol. 10, no. 3, p. 106, Sep. 2021, doi: 10.3390/robotics10030106.

[5] C. Getson and G. Nejat, “The Robot Screener Will See You Now: A Socially Assistive Robot for COVID-19 Screening in Long-Term Care Homes,” in 2022 31st IEEE International Conference on Robot and Human Interactive Communication (RO-MAN), Napoli, Italy: IEEE, Aug. 2022, pp. 672–677. doi: 10.1109/RO-MAN53752.2022.9900620.

[6] J. Wang, W. P. Chan, P. Carreno-Medrano, A. Cosgun, and E. Croft, “Metrics for Evaluating Social Conformity of Crowd Navigation Algorithms,” in 2022 IEEE International Conference on Advanced Robotics and Its Social Impacts (ARSO), May 2022, pp. 1–6. doi: 10.1109/ARSO54254.2022.9802981.

[7] P. T. Singamaneni et al., “A survey on socially aware robot navigation: Taxonomy and future challenges,” The International Journal of Robotics Research, p. 02783649241230562, Feb. 2024, doi: 10.1177/02783649241230562.

[8] C. Getson and G. Nejat, “The adoption of socially assistive robots for long-term care: During COVID-19 and in a post-pandemic society,” Healthc Manage Forum, vol. 35, no. 5, pp. 301–309, Sep. 2022, doi: 10.1177/08404704221106406.

[9] C. Mavrogiannis et al., “Core Challenges of Social Robot Navigation: A Survey,” J. Hum.-Robot Interact., vol. 12, no. 3, pp. 1–39, Sep. 2023, doi: 10.1145/3583741.

[10] R. Mirsky, X. Xiao, J. Hart, and P. Stone, “Conflict Avoidance in Social Navigation – a Survey,” Dec. 28, 2022, arXiv: arXiv:2106.12113. Accessed: Apr. 05, 2024. [Online]. Available: http://arxiv.org/abs/2106.12113

[11] W. Wang, R. Wang, L. Mao, and B.-C. Min, “NaviSTAR: Socially Aware Robot Navigation with Hybrid Spatio-Temporal Graph Transformer and Preference Learning,” Sep. 26, 2023, arXiv: arXiv:2304.05979. Accessed: Mar. 31, 2024. [Online]. Available: http://arxiv.org/abs/2304.05979

[12] A. J. Sathyamoorthy, U. Patel, M. Paul, N. K. S. Kumar, Y. Savle, and D. Manocha, “CoMet: Modeling Group Cohesion for Socially Compliant Robot Navigation in Crowded Scenes,” IEEE Robot. Autom. Lett., vol. 7, no. 2, pp. 1008–1015, Apr. 2022, doi: 10.1109/LRA.2021.3135560.

[13] V. Narayanan, B. M. Manoghar, R. P. RV, and A. Bera, “EWareNet: Emotion Aware Human Intent Prediction and Adaptive Spatial Profile Fusion for Social Robot Navigation,” Mar. 07, 2023, arXiv: arXiv:2011.09438. Accessed: Apr. 08, 2024. [Online]. Available: http://arxiv.org/abs/2011.09438

[14] L. Kästner, J. Li, Z. Shen, and J. Lambrecht, “Enhancing Navigational Safety in Crowded Environments using Semantic-Deep-Reinforcement-Learning-based Navigation,” 2021, doi: 10.48550/ARXIV.2109.11288.

[15] N. Hirose, D. Shah, A. Sridhar, and S. Levine, “SACSoN: Scalable Autonomous Control for Social Navigation,” IEEE Robot. Autom. Lett., vol. 9, no. 1, pp. 49–56, Jan. 2024, doi: 10.1109/LRA.2023.3329626.

[16] E. Escudie, L. Matignon, and J. Saraydaryan, “Attention Graph for Multi-Robot Social Navigation with Deep Reinforcement Learning,” Jan. 31, 2024, arXiv: arXiv:2401.17914. Accessed: Jul. 29, 2024. [Online]. Available: http://arxiv.org/abs/2401.17914

[17] J. Liang, U. Patel, A. J. Sathyamoorthy, and D. Manocha, “Crowd-Steer: Realtime Smooth and Collision-Free Robot Navigation in Densely Crowded Scenarios Trained using High-Fidelity Simulation,” in Proceedings of the Twenty-Ninth International Joint Conference on Artificial Intelligence, Yokohama, Japan: International Joint Conferences on Artificial Intelligence Organization, Jul. 2020, pp. 4221–4228. doi: 10.24963/ijcai.2020/583.

[18] J. Xu, W. Zhang, J. Cai, and H. Liu, “SafeCrowdNav: safety evaluation of robot crowd navigation in complex scenes,” Front. Neurorobot., vol. 17, p. 1276519, Oct. 2023, doi: 10.3389/fnbot.2023.1276519.

[19] A. H. Raj et al., “Rethinking Social Robot Navigation: Leveraging the Best of Two Worlds,” Mar. 09, 2024, arXiv: arXiv:2309.13466. Accessed: Apr. 05, 2024. [Online]. Available: http://arxiv.org/abs/2309.13466

[20] B. Panigrahi, A. H. Raj, M. Nazeri, and X. Xiao, “A Study on Learning Social Robot Navigation with Multimodal Perception,” Sep. 21, 2023, arXiv: arXiv:2309.12568. Accessed: Apr. 05, 2024. [Online]. Available: http://arxiv.org/abs/2309.12568

[21] W. Wang, L. Mao, R. Wang, and B.-C. Min, “SRLM: Human-in-Loop Interactive Social Robot Navigation with Large Language Model and Deep Reinforcement Learning,” Mar. 22, 2024, arXiv: arXiv:2403.15648. Accessed: Mar. 31, 2024. [Online]. Available: http://arxiv.org/abs/2403.15648

[22] D. Song, J. Liang, A. Payandeh, X. Xiao, and D. Manocha, “Socially Aware Robot Navigation through Scoring Using Vision-Language Models,” Mar. 29, 2024, arXiv: arXiv:2404.00210. Accessed: Apr. 05, 2024. [Online]. Available: http://arxiv.org/abs/2404.00210

[23] C. Weinrich, M. Volkhardt, E. Einhorn, and H.-M. Gross, “Prediction of human collision avoidance behavior by lifelong learning for socially compliant robot navigation,” in 2013 IEEE International Conference on Robotics and Automation, Karlsruhe, Germany: IEEE, May 2013, pp. 376–381. doi: 10.1109/ICRA.2013.6630603.

[24] I. Okunevich, A. Lombard, T. Krajnik, Y. Ruichek, and Z. Yan, “Online Context Learning for Socially-compliant Navigation,” Jun. 17, 2024, arXiv: arXiv:2406.11495. Accessed: Jul. 16, 2024. [Online]. Available: http://arxiv.org/abs/2406.11495

[25] J. Redmon and A. Farhadi, “YOLOv3: An Incremental Improvement,” Apr. 08, 2018, arXiv: arXiv:1804.02767. Accessed: Sep. 14, 2024. [Online]. Available: http://arxiv.org/abs/1804.02767

[26] H. Karnan et al., “Socially Compliant Navigation Dataset (SCAND): A Large-Scale Dataset of Demonstrations for Social Navigation,” Jun. 08, 2022, arXiv: arXiv:2203.15041. Accessed: Apr. 05, 2024. [Online]. Available: http://arxiv.org/abs/2203.15041

[27] D. M. Nguyen, M. Nazeri, A. Payandeh, A. Datar, and X. Xiao, “Toward Human-Like Social Robot Navigation: A Large-Scale, Multi-Modal, Social Human Navigation Dataset,” Aug. 09, 2023, arXiv: arXiv:2303.14880. Accessed: Apr. 05, 2024. [Online]. Available: http://arxiv.org/abs/2303.14880

[28] T. Schreiter et al., “THÖR-MAGNI: A Large-scale Indoor Motion Capture Recording of Human Movement and Robot Interaction,” Mar. 14, 2024, arXiv: arXiv:2403.09285. Accessed: Sep. 13, 2024. [Online]. Available: http://arxiv.org/abs/2403.09285

[29] W. Chen, O. Mees, A. Kumar, and S. Levine, “Vision-Language Models Provide Promptable Representations for Reinforcement Learning,” Feb. 13, 2024, arXiv: arXiv:2402.02651. Accessed: Apr. 12, 2024. [Online]. Available: http://arxiv.org/abs/2402.02651

[30] OpenAI et al., “GPT-4 Technical Report,” Mar. 04, 2024, arXiv: arXiv:2303.08774. Accessed: Jul. 29, 2024. [Online]. Available: http://arxiv.org/abs/2303.08774

[31] S. Kim, H. Jeon, J. Choi, and D. Kum, “Diverse Multiple Trajectory Prediction Using a Two-stage Prediction Network Trained with Lane Loss,” IEEE Robot. Autom. Lett., vol. 8, no. 4, pp. 2038–2045, Apr. 2023, doi: 10.1109/LRA.2022.3231525.

[32] A. Radford et al., “Learning Transferable Visual Models From Natural Language Supervision,” Feb. 26, 2021, arXiv: arXiv:2103.00020. Accessed: Jun. 23, 2024. [Online]. Available: http://arxiv.org/abs/2103.00020

[33] A. Vaswani et al., “Attention Is All You Need,” Aug. 01, 2023, arXiv: arXiv:1706.03762. Accessed: Jun. 26, 2024. [Online]. Available: http://arxiv.org/abs/1706.03762

[34] B. Zhang, P. Zhang, X. Dong, Y. Zang, and J. Wang, “Long-CLIP: Unlocking the Long-Text Capability of CLIP,” May 23, 2024, arXiv: arXiv:2403.15378. Accessed: May 29, 2024. [Online]. Available: http://arxiv.org/abs/2403.15378

[35] J. Shlens, “A Tutorial on Principal Component Analysis,” Apr. 03, 2014, arXiv: arXiv:1404.1100. Accessed: Jul. 29, 2024. [Online]. Available: http://arxiv.org/abs/1404.1100

[36] L. Wang, L. Xiang, Y. Wei, Y. Wang, and Z. He, “CLIP model is an Efficient Online Lifelong Learner,” May 23, 2024, arXiv: arXiv:2405.15155. Accessed: Jun. 19, 2024. [Online]. Available: http://arxiv.org/abs/2405.15155

[37] Y. Zhou and O. Tuzel, “VoxelNet: End-to-End Learning for Point Cloud Based 3D Object Detection,” in 2018 IEEE/CVF Conference on Computer Vision and Pattern Recognition, Salt Lake City, UT, USA: IEEE, Jun. 2018, pp. 4490–4499. doi: 10.1109/CVPR.2018.00472.

[38] K. He, X. Zhang, S. Ren, and J. Sun, “Deep Residual Learning for Image Recognition,” Dec. 10, 2015, arXiv: arXiv:1512.03385. Accessed: Jul. 29, 2024. [Online]. Available: http://arxiv.org/abs/1512.03385

[39] S. Casas et al., “DeTra: A Unified Model for Object Detection and Trajectory Forecasting,” Jun. 13, 2024, arXiv: arXiv:2406.04426. Accessed: Jun. 15, 2024. [Online]. Available: http://arxiv.org/abs/2406.04426

[40] Kiam Heong Ang, G. Chong, and Yun Li, “PID control system analysis, design, and technology,” IEEE Trans. Contr. Syst. Technol., vol. 13, no. 4, pp. 559–576, Jul. 2005, doi: 10.1109/TCST.2005.847331.

[41] K. Gandhi, J.-P. Fränken, T. Gerstenberg, and N. D. Goodman, “Understanding Social Reasoning in Language Models with Language Models,” Dec. 04, 2023, arXiv: arXiv:2306.15448. Accessed: Sep. 15, 2024. [Online]. Available: http://arxiv.org/abs/2306.15448

[42] I. Loshchilov and F. Hutter, “SGDR: Stochastic Gradient Descent with Warm Restarts,” May 03, 2017, arXiv: arXiv:1608.03983. Accessed: Aug. 23, 2024. [Online]. Available: http://arxiv.org/abs/1608.03983

[43] I. Loshchilov and F. Hutter, “Decoupled Weight Decay Regularization,” Jan. 04, 2019, arXiv: arXiv:1711.05101. Accessed: Aug. 23, 2024. [Online]. Available: http://arxiv.org/abs/1711.05101

[44] D. Kraft, “Computing the Hausdorff Distance of Two Sets from Their Signed Distance Functions,” Int. J. Comput. Geom. Appl., vol. 30, no. 01, pp. 19–49, Mar. 2020, doi: 10.1142/S0218195920500028.

[45] N. Hirose, D. Shah, K. Stachowicz, A. Sridhar, and S. Levine, “SELFI: Autonomous Self-Improvement with Reinforcement Learning for Social Navigation,” Mar. 01, 2024, arXiv: arXiv:2403.00991. Accessed: Mar. 13, 2024. [Online]. Available: http://arxiv.org/abs/2403.00991

[46] C. Yu et al., "The Surprising Effectiveness of PPO in Cooperative, Multi-Agent Games," Nov. 04, 2022, arXiv: arXiv:2103.01955. Accessed: Sep. 09, 2024. [Online]. Available: http://arxiv.org/abs/2103.01955